Received: 8 February 2024 | Revised: 9 April 2024 | Accepted: 26 April 2024

DOI: 10.1002/pld3.592

RESEARCH ARTICLE

A chemical genetic screen with the EXO70 inhibitor Endosidin2 uncovers potential modulators of exocytosis in Arabidopsis

Xiaohui Li[1,2] | Diwen Wang[1,2] | Xianglin Yin[3] | Mingji Dai[3,4] | Christopher J. Staiger[1,2,5] | Chunhua Zhang[1,2†]

[1]Department of Botany and Plant Pathology, Purdue University, West Lafayette, Indiana, USA

[2]Center for Plant Biology, Purdue University, West Lafayette, Indiana, USA

[3]Department of Chemistry, Purdue University, West Lafayette, Indiana, USA

[4]Department of Chemistry, Emory University, Atlanta, Georgia, USA

[5]Department of Biological Sciences, Purdue University, West Lafayette, Indiana, USA

Correspondence
Christopher J. Staiger, Department of Botany and Plant Pathology, Purdue University, West Lafayette, IN 47907, USA.
Email: staiger@purdue.edu

Present address
Mingji Dai, Department of Chemistry, Emory University, Atlanta, Georgia, USA.

Funding information
This research was primarily supported by start-up funds awarded to CZ from Purdue University Office of the Provost. XL was partially supported by a research assistantship awarded by the Purdue Center for Plant Biology and a Bilsland Fellowship awarded by the Purdue College of Agriculture.

Abstract

Exocytosis plays an essential role in delivering proteins, lipids, and cell wall polysaccharides to the plasma membrane and extracellular spaces. Accurate secretion through exocytosis is key to normal plant development as well as responses to biotic and abiotic stresses. During exocytosis, an octameric protein complex named the exocyst facilitates the tethering of secretory vesicles to the plasma membrane. Despite some understanding of molecular and cellular aspects of exocyst function obtained through reverse genetics and direct interaction assays, knowledge about upstream modulators and genetic interactors remains limited. Traditional genetic screens encounter practical issues in exocyst subunit mutant backgrounds, such as lethality of certain knockout mutants and/or potential redundancy of EXO70 homologs. To address these challenges, this study leverages the tunable and reversible nature of chemical genetics, employing Endosidin2 (ES2)—a synthetic inhibitor of EXO70—for a large-scale chemical genetic mutant screen in Arabidopsis. This approach led to the identification of 70 ES2-hypersensitive mutants, named *es2s*. Through a whole-genome sequencing-based mapping strategy, 14 nonallelic *es2s* mutants were mapped and the candidate mutations reported here. In addition, T-DNA insertion lines were tested as alternative alleles to identify causal mutations. We found that T-DNA insertion alleles for *DCP5*, *VAS1/ISS1*, *ArgJ*, and *MEF11* were hypersensitive to ES2 for root growth inhibition. This research not only offers new genetic resources for systematically identifying molecular players interacting with the exocyst in Arabidopsis but also enhances understanding of the regulation of exocytosis.

KEYWORDS
chemical genetic screen, Endosidin2 (ES2), exocyst, exocytosis, hypersensitive mutant screen, mutant mapping

† Deceased.

1 | INTRODUCTION

Exocytosis is an essential process for eukaryotic organisms that encompasses the packaging of cargo into secretory vesicles at the trans-Golgi network (TGN) as well as their transport, tethering, docking, and fusion with the plasma membrane (PM) (Aniento et al., 2022; Battey et al., 1999). In plants, exocytosis is important for numerous key functions by delivering proteins to the PM to fine tune the PM proteome composition, as well as by delivering lipids, polysaccharides, and other substances to the cell surface and extracellular spaces (Zhang, Xing, & Lin, 2019). Exocytosis delivers PM proteins with various functions, for instance, the PIN-FORMED (PIN) proteins that are required for auxin transport (Drdová et al., 2013), the cellulose synthase complex (CSC) that is required for cell wall formation (Zhang et al., 2021; Zhang, Cai, & Staiger, 2019; Zhu et al., 2018; Zhu & McFarlane, 2022), and the pathogenesis-related (PR) proteins that are secreted into the apoplast upon salicylic acid (SA) treatment or pathogen infection (Zavaliev et al., 2013).

During exocytosis, a conserved octameric protein complex named the exocyst facilitates the tethering of secretory vesicles with the PM (Elias et al., 2003; Heider & Munson, 2012). The exocyst complex consists of eight subunits, SEC3, SEC5, SEC6, SEC8, SEC10, SEC15, EXO70, and EXO84 (Mei et al., 2018). In plants, the EXO70 subunit comprises a large protein family, with 23 paralogs in Arabidopsis (Cvrčková et al., 2012). Among the EXO70 paralogs in Arabidopsis, EXO70A1 is the most studied. A knock-out mutant for *exo70A1* has severe growth defects (Zhang et al., 2016), presenting challenges for forward genetic screens.

The auxin-efflux carrier protein PIN2 is polarized to the apical PM of root epidermal cells at the root tip (Xu & Scheres, 2005). The exocyst complex facilitates the delivery and recycling of PIN2 at the PM (Drdová et al., 2013). Moreover, *exo70A1* displayed compromised polar auxin transport in roots and abnormal retention of PIN2 in intracellular compartments (Drdová et al., 2013). Given the important role of PIN2 in auxin transport and its polar PM distribution with minimal cytoplasm localization, it is frequently used as a representative cargo protein for membrane protein trafficking studies (Friml, 2010; Ischebeck et al., 2014; Kleine-Vehn et al., 2011; Luschnig & Vert, 2014).

Previous studies identified a synthetic molecule, Endosidin2 (ES2), that interferes with membrane trafficking by targeting the EXO70A1 subunit of the exocyst (Drakakaki et al., 2011; Zhang et al., 2016). ES2 disrupts the proper PM localization of EXO70 in Arabidopsis and mammalian cells (Li et al., 2023; Zhang et al., 2016) and causes the formation of small PIN2 aggregation compartments (PIN2 bodies) in the cytoplasm (Lešková et al., 2020; Li et al., 2023). A 2-h ES2 treatment alters the PM proteome of Arabidopsis root cells and markedly reduces the abundance of a plethora of PM proteins important for plant growth and signal transduction (Li et al., 2023).

As an exocyst inhibitor, ES2 has synergistic effects with genetic mutations related to exocytosis in Arabidopsis, including *scd1* and *scd2*, as well as *nerd1* (Cole et al., 2018; Mayers et al., 2017). STOMATAL CYTOKINESIS DEFECTIVE1 (SCD1) and SCD2 form the SCD complex that physically and functionally interacts with exocyst subunits (Mayers et al., 2017). Mutant plants of *scd1* and *scd2* display a hypersensitive response to ES2 for inhibition of root elongation and PIN2 body formation. *NEW ENHANCER OF ROOT DWARFISM1* (*NERD1*) was identified in a forward genetic screen as an enhancer of *sec8-6*, a weak allele of exocyst mutants (Cole et al., 2018). *NERD1* encodes a Golgi-resident transmembrane protein of unknown function and genetically interacts with weak alleles of *SEC8* and *EXO70A1*. Seedlings of *nerd1-2* also exhibit an ES2-hypersensitive phenotype for root growth inhibition.

Studies of plant exocytosis achieved substantial advances using reverse genetics to reveal the role of Rho GTPases (Chen & Friml, 2014), soluble NSF attachment protein receptor (SNARE) proteins (Larson et al., 2020), and Myosin XI motors (Zhang et al., 2021; Zhang, Cai, & Staiger, 2019). In spite of that, a systematic understanding of exocytosis still needs to be fulfilled, including identification of regulators and genetic interactors of the exocyst complex. To identify novel players and regulators of exocytosis, a systematic approach to identify mutants with modest exocytosis defects is needed. However, traditional forward genetic screens face challenges in the exocyst mutant background, because of the seedling lethal phenotype associated with the homozygous *exo70A1* knockout line, and the abundance of *EXO70* paralogs. Thus, we sought to develop a chemical genetics approach that is tunable and reversible. Leveraging the effects of ES2 as an EXO70 inhibitor, as well as its ability to cause synergistic effects with exocytosis-related genetic mutations, we employed it as a sensitizer for a large-scale chemical genetic screen to identify ES2-hypersensitive mutants. In this study, we generated a large collection of ethyl methanesulfonate (EMS)-induced mutants, mapped these mutants, documented the single nucleotide polymorphisms (SNPs) in each mutant, and tested alternative alleles for ES2-hypersensitivity.

2 | MATERIALS AND METHODS

2.1 | Plant growth conditions

pPIN2::PIN2-GFP;eir1 (referred to as *PIN2-GFP* hereafter; Xu & Scheres, 2005) was used for EMS mutagenesis. The T-DNA insertion lines used in this study were ordered from the Arabidopsis Biological Resources Center (ABRC; Ohio State University, Ohio, USA). All Arabidopsis lines were in *Col-0* ecotype background. For seed propagation and crosses, plants were grown in pots filled with propagation mix, placed on light racks in growth rooms at 23°C and 24-h continuous light. For root growth assays, seeds were surface sterilized and sowed on half-strength Murashige and Skoog (½ MS) media with vitamins (Cat# MSP09; Caisson Labs, Smithfield, UT, USA), 1% (w/v) sucrose, and 0.8% (w/v) agar (Fisher Scientific, Waltham, MA, USA), supplemented with DMSO (mock) or various concentrations of ES2. Plates were placed in vertical orientation in a growth chamber (Percival Scientific, Perry, IA, USA) under 24-h continuous light of 130 μmol m^{-2} s^{-1} at 23°C.

2.2 | Chemicals

Endosidin2 [(E)-3-Fluoro-N′-(4-hydroxy-3-iodo-5-methoxybenzylidene)-benzohydrazide] (Molecular weight 414.17 Da) was synthesized from the reaction between3-fluorophenylhydrazide and 5-iodovanillin at the Department of Chemistry, Purdue University. A 40-mM stock solution was prepared by dissolving 82.8-mg ES2 in DMSO for a final volume of 5 mL. The ES2 powder and stock solution were both stored at −20°C.

2.3 | EMS mutagenesis and mutant screen

To obtain mutagenized seed pools, *PIN2-GFP* seeds were soaked in 0.4% EMS solution overnight following a published protocol (Kim et al., 2006). The mutagenized M1 seeds were grown in trays in a dedicated walk-in growth chamber to prevent seed contamination. M2 seeds were obtained through selfing and were collected in pools.

For the first round of ES2-hypersensitive screen, approximately 100,000 M2 seeds were sterilized and sowed on plates containing solid ½ MS media supplemented with 15- or 20-μM ES2 in multiple batches, together with wild-type *PIN2-GFP* as control. After 5 days, seedlings with short roots were carefully transferred to plates without ES2 and grown for three more days. Approximately 1200 seedlings with restored root growth were selected to transfer to soil, allowed to self to obtain M3 seeds, and individually harvested.

For the second round of screening, approximately 1200 individual M3 lines were sowed on ½ MS plates containing 0-, 15-, or 25-μM ES2 and grown in the light chamber simultaneously, with wild-type *PIN2-GFP* as control. The M3 lines displaying a more dramatic response to low-dose ES2, compared with wild type, were selected as *es2s* mutants.

2.4 | Mutant mapping

To obtain mapping populations, *es2s* mutants were outcrossed to *Ler* ecotype and/or backcrossed to wild-type *PIN2-GFP*. The F_1 generations were grown in soil and selfed to obtain segregating F_2 populations. For each of the mutant lines, at least 600 F_2 seeds were sowed on plates containing 15- or 20-μM ES2. After 5 days of growth, seedlings with short roots were carefully transferred to plates without ES2. Seedlings with restored root growth were selected and pooled. Seedlings with unrestored root growth were discarded. Genomic DNA was extracted from the pooled seedlings with the CTAB method (Wilson et al., 2018).

DNA library preparation and whole-genome sequencing of the F_2 population were performed by the Purdue Genomics Core Facility or by Novogene (Sacramento, CA, USA). Paired-end 150 bp reads were generated with the Illumina HiSeq platform. The reads were mapped to Arabidopsis TAIR10 genome (https://www.arabidopsis.org/download_files/Genes/TAIR10_genome_release/TAIR10_chromosome_files/TAIR10_chr_all.fas.gz) with Bowtie 2 (Langmead & Salzberg, 2012) and sorted with SAMtools (Ver 1.10) (Li et al., 2009). The variants were called with an early version of SAMtools (Ver 0.1.16), because the output format from newer versions of SAMtools were not compatible with downstream SNP annotation analyses. For outcrossed populations, the histogram of genetic variants density was generated by Next-Generation EMS mutation Mapping tool (NGM) (Austin et al., 2011, 2014). The SNPs were annotated by NGM as well. Gene name and descriptions were obtained from TAIR (https://www.arabidopsis.org). For backcrossed populations, the SNPs were plotted with a custom R script to identify the chromosomal interval containing the causal mutation.

3 | RESULTS

3.1 | ES2 inhibits Arabidopsis root growth in a dose-dependent manner

To optimize the concentration of ES2 before applying it to a large-scale hypersensitive chemical genetic screen, ES2 dose–response curves for Arabidopsis root growth inhibition were generated. Seedlings of *Col-0* and *PIN2-GFP* were grown vertically on plates containing ½ MS solid media, supplemented with different concentrations of ES2. Modest root growth inhibition was observed with 15- to 25-μM ES2 treatment for *PIN2-GFP* and *Col-0* (Figure 1).

3.2 | Identification of ES2-hypersensitive mutants

To create a mutant population suitable for this study and to allow investigations of subcellular phenotypes, we opted to perform mutagenesis in the background of a widely used membrane trafficking cargo marker, *PIN2-GFP* (Xu & Scheres, 2005). The seeds were mutagenized with EMS treatment and propagated through self-crossing to get M2 population pools carrying homozygous mutations. Subsequently, a two-round screening strategy to identify ES2-hypersensitive mutants was employed (Figure 2a). For the primary screen, approximately 100,000 M2 seeds were sowed on ½ MS solid media containing low-dose (15–20 μM) ES2 and screened for seedlings with short roots. To eliminate mutants with root growth defects that were not related to ES2 treatment, seedlings with short roots were transferred to ½ MS solid media without ES2 and allowed to recover. Seedlings for which root growth was not restored after transferring to ES2-free media were discarded. Approximately 1200 seedlings with restored root growth were selected to self-propagate for another generation (M3), with seeds harvested individually from each plant. The M3 seedlings of each individual line were grown on ½ MS solid media containing either no ES2, 15-μM ES2, or 25-μM ES2 as a secondary screen. At this stage, mutant lines with an obvious ES2-hypersensitive response were selected, which responded to low-dose ES2 more dramatically than wild-type *PIN2-GFP*. Collectively, 70 ES2-hypersensitive mutant lines were identified and named *es2s* (*ES2-SENSITIVE* mutants). Given the substantial number of mutant

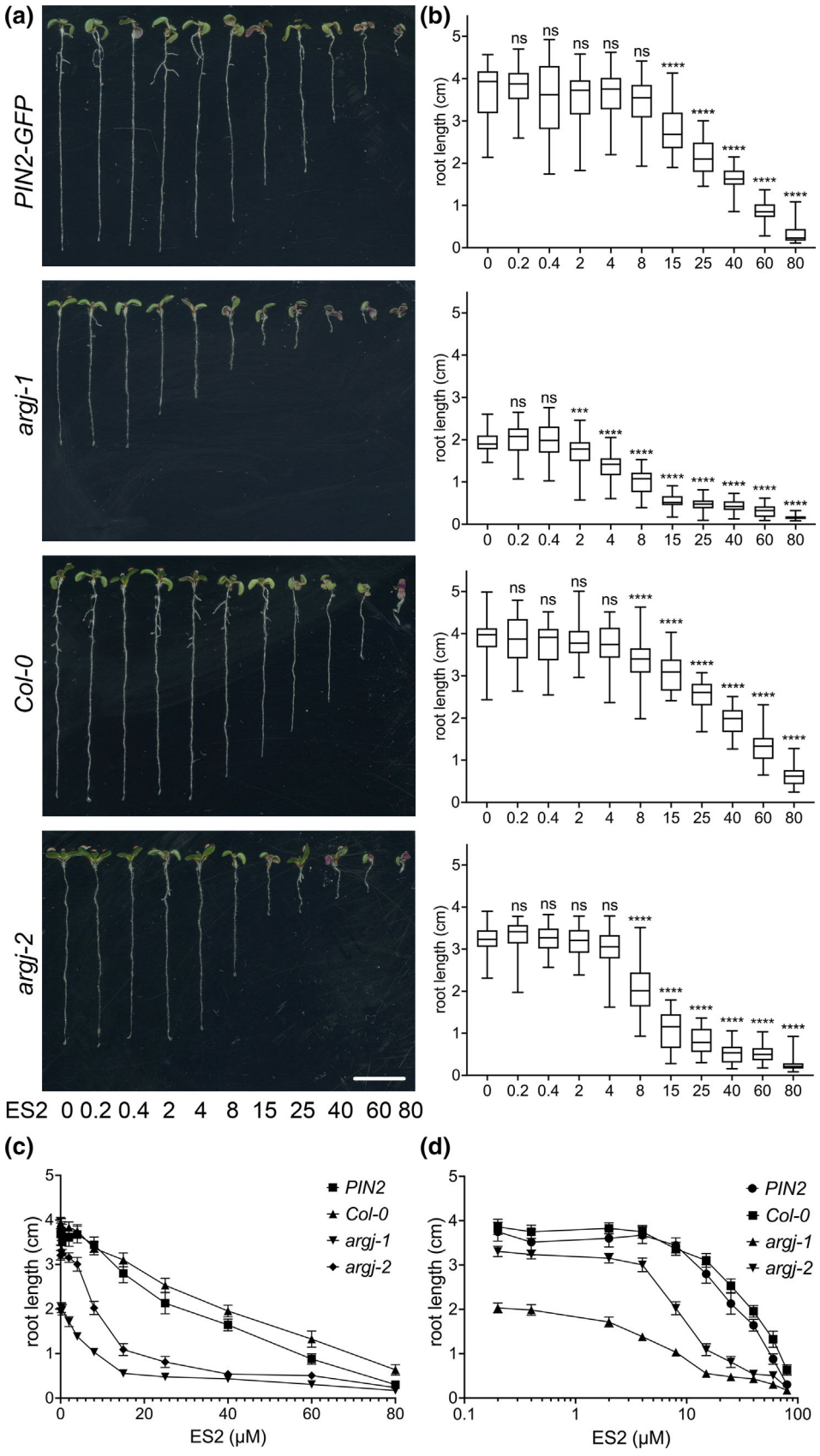

FIGURE 1 Endosidin2 (ES2) inhibits Arabidopsis root growth in a dose-dependent manner. (a) Seven-day-old light-grown seedlings of *PIN2-GFP* and *Col-0* grown on solid ½ MS media containing various concentrations of ES2. Representative seedlings are displayed. Scale bar = 1 cm. (b) Growth curve of root lengths for seedlings after ES2 treatment. (c) Box plot of root lengths for 7-day-old seedlings with ES2 dose series treatment, with whiskers displaying the minimum and maximum root length in each group. Statistical analysis was performed with one-way ANOVA, with Dunnett multiple comparison with the control group. ***denotes $p < 0.001$, **** denotes $p < 0.0001$, ns denotes not significant. $N = 45–60$ seedlings for *PIN2-GFP*, and 58–74 seedlings for *Col-0*, from 3 biological replicates.

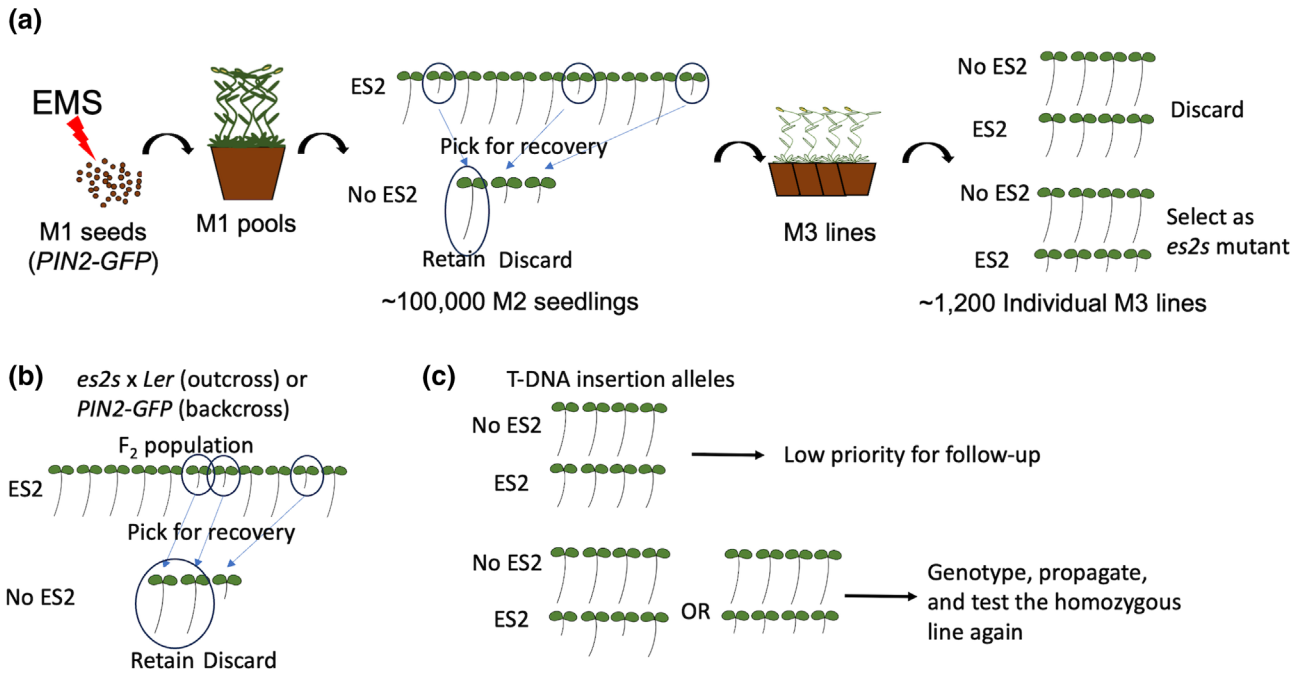

FIGURE 2 Schematics of ES2-hypersensitive mutant screening, mapping, and alternative allele testing. (a) Identification of ES2-hypersensitive (*es2s*) mutants with a two-round screening strategy. In the first round, about 100,000 M2 seedlings were screened for ES2-sensitivity. Seedlings with reduced growth in the presence of ES2, but with normal growth after recovery on plates without ES2 were selected for propagation. In the second round, individual M3 lines were sowed on plates with no ES2 and low dose ES2. The lines displayed hypersensitive response to low dose ES2 were selected as *es2s* mutants. (b) The *es2s* mutant lines were outcrossed to *Ler* ecotype and/or backcrossed to *PIN2-GFP* for mapping. Seedlings displaying ES2-hypersensitive response from the F_2 population from each line were pooled for whole genome sequencing. Computational genomics analysis was used to identify the nonrecombinant regions in the pooled samples, which harbored the causal mutations. (c) A strategy of using T-DNA insertion lines as alternative alleles to identify the causal mutation was used. Multiple SNPs were present in the nonrecombinant regions for each of the *es2s* mutants. T-DNA insertion lines were ordered and tested for ES2-hypersensitivity. Due to the substantial number of SNPs and labor constraints, only T-DNA insertion lines with ES2-hypersensitive response were followed up.

TABLE 1 Summary of ES2-hypersensitive mutants.

ES2 hypersensitive mutant	Nonrecombinant region	ES2 hypersensitive mutant	Nonrecombinant region
es2s-1-2	Likely to be left arm of chr 1, 0–10 M	*es2s-11-9*	Not identified
es2s-2-19	Left arm of chr 1, 5.6–10.5 M, might be same as *es2s-18-1*	*es2s-12-5*	Not clear, right terminus of chr 2, 15–19.7 M
es2s-2-29	Left arm of chr 1, 6.8–10.8 M	*es2s-15-9*	Right arm of chr 4, 6.8–10.6 M, same as *16-5*
es2s-3-4	Not identified	*es2s-15-12*	Right arm of chr 2, 14.0–17.5 M
es2s-3-6	Right arm of chr 5, 16–20.5 M	*es2s-16-5*	Right arm of chr 4, 6.8–10.6 M, same region as *15-9*
es2s-6-3	Chr 1, left arm, 8.0–11.0 M	*es2s-16-10*	Not identified
es2s-6-4	Same as *es2s-6-3*, chr 1, left arm, 8.0–11.0 M	*es2s-18-1*	Left arm of chr 1, 7.0–10.0 M
es2s-6-7	Same as *es2s-6-3*, Chr 1, 8.0–11.0 M	*es2s-19-2*	Right terminus of chr 1, same region as *10-2*, 26–31 M, 28.5 M as center
es2s-6-13	Chr 3, right arm, 18.5–23.5 M	*es2s-19-11*	Left arm of chr 5, 0–6 M, 4 M as center
es2s-10-2	Right terminus of chr 1, 26.5–30.4 M	*es2s-20-4*	Not identified
es2s-10-7	Not identified	*es2s-23-1*	Not identified
es2s-10-16	Chr5 right arm, 19–24.5 M, centers 22.6 M	*es2s-33-7*	Chr 1, 6–10 M

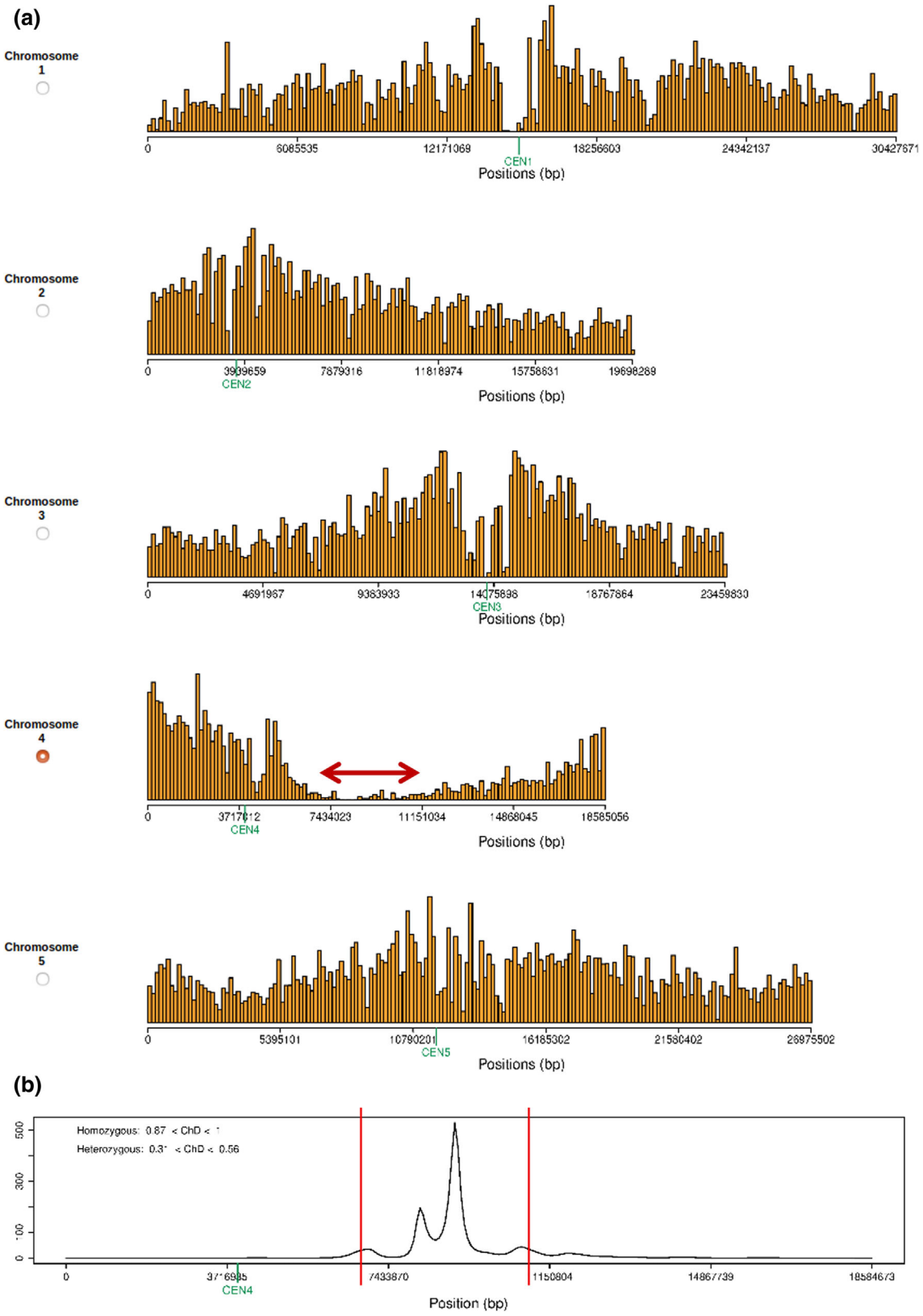

FIGURE 3 *es2s-16-5* maps to the right arm of chromosome 4, between 6.8 and 10.6 Mbp. (a) Binned histogram of genetic variation density along each chromosome of pooled seedlings with ES2-hypersensitive phenotype from F_2 population of *es2s-16-5* × *Ler*. A nonrecombinant interval was identified at the right arm of chromosome 4. (b) Homozygous/heterozygous signal ratio along chromosome 4. The region surrounding the signal peak was most likely to harbor the causal mutation.

TABLE 2 Candidate SNPs in *es2s-15-9* and *es2s-16-5*.

Mutant: *es2s-15-9* and *es2s-16-5*													
Chr	**Position**	**Ref. base**	**SNP base**	**Depth**	**Discordantchastity**	**Accession**	**Tag**	**Strand**	**Ref. codon**	**SNP codon**	**AA change**	**BLOSUM100**	**Gene name/annotation**
4	8135417	C	T	103	0.94	AT4G14120.1	CDS	+	ACC	ATC	T → I	-3	Hypothetical protein
4	8515097	G	A	113	1	AT4G14850.1	CDS	+	GGA	GAA	G384E	-6	*LOI1*, *LOVASTATIN INSENSITIVE 1*, *MEF11*, *MITOCHONDRIAL RNA EDITING FACTOR 11*, Pentatricopeptide repeat (PPR) superfamily protein
4	8995734	G	A	84	0.99	AT4G15830.1	CDS	−	CGC	TGC	R → C	−8	ARM repeat superfamily protein, contains CLASP N motif, CLASPs are widely conserved microtubule plus-end-tracking proteins that regulate the stability of dynamic microtubules
4	9050099	G	A	138	0.99	AT4G15970.1	CDS	+	CGC	CAC	R → H	−1	Nucleotide-diphospho-sugar transferase family protein
4	9620416	G	A	124	0.97	AT4G17140.1	CDS	−	TCT	TTT	S → F	−5	Pleckstrin homology (PH) domain-containing protein, can be aligned to yeast VPS13 and VPS62, 1580-1596 and 1696-1718 is likely to be TM domain
4	10413149	G	A	103	0.95	AT4G19010.1	Cryptic splice site (5 bp)						AMP-dependent synthetase and ligase family protein. It functions in the biosynthesis of ubiquinone (Coenzyme Q).

lines recovered, we proceeded to whole-genome sequencing (WGS)-based mapping, without performing pairwise crosses to test for allelism.

3.3 | Mapping of *es2s* mutants

To map the genes responsible for ES2-hypersensitive phenotypes, *es2s* lines were outcrossed to *Ler* ecotype and/or backcrossed to wild-type *PIN2-GFP* (Figure 2b). In each of the outcrossed or backcrossed F_2 populations, seedlings with short roots on plates containing low-dose ES2 were selected and pooled for WGS. Through WGS mapping analysis and binning of the naturally present genomic variations between *Col-0* and *Ler*, we identified the nonrecombinant region on the chromosome in which the likely causal mutation was located, as summarized in Table 1, with sequencing statistics detailed in Table S1. The chromosomal mapping results for each *es2s* mutant are displayed in Figure 3 and Figures S1–S18. The SNPs caused by EMS-mutagenesis in these nonrecombinant regions were identified and annotated, as summarized in Table 2 and Tables S2–S13. For each *es2s* mutant, there were four to 24 candidate SNPs in the nonrecombinant interval. To date, we attempted to map 24 *es2s* mutants (Table S1), and 14 were identified to be nonallelic mutants by WGS-based mapping (Table 1).

3.4 | Summary of candidate genes for each *es2s* mutant

es2s-15-9 and *es2s-16-5* were both mapped to the right arm of chromosome 4, in the 6.8- to 10.6-Mbp interval (Figure 3 and Figure S13). The same set of six SNPs were identified at this interval by SNP calling and annotation analysis (Table 2). Notably, a unique SNP at position 8515097 caused a G384E single amino acid replacement mutation in MEF11/LOI1 (MITOCHONDRIA RNA EDITING FACTOR 11, or LOVASTATIN INSENSITIVE 1). There were also SNPs in AT4G15830 and AT4G17140, which encode a protein involved in microtubule cytoskeleton organization and a pleckstrin homology (PH) domain-containing protein, respectively.

es2s-1-2 was roughly mapped to a wide interval at the left arm of chromosome 1 (Figure S1). The mapping was not clear and did not give enough confidence to identify causal mutations. Given the low mapping resolution for *es2s-1-2* and the substantial number of SNPs in this large interval, we did not include a table of SNPs for this mutant.

es2s-2-19 was mapped to the left arm of chromosome 1, between position 5.6–10.5 Mbp (Figure S2). In this interval, there were SNPs in six candidate genes as listed in Table S2. Notably, there was a C to T SNP at Chr1: 6047688, causing an A1220V single amino acid replacement in MYOSIN XI-1 (Table S2).

es2s-2-29 was mapped to the left arm of chromosome 1, between position 6.8–10.8 Mbp (Figure S3). Although this was the same interval as *es2s-2-19*, the SNPs within this interval were different. The nonrecombinant region on chromosome 1 was not clean, with some contents inherited from *Ler*. In this interval, there were SNPs in 14 candidate genes, as listed in Table S3. Notably, mutations in AT1G24150 (*FORMIN HOMOLOGUE 4*, *FH4*) and AT1G25360 (*ORGANELLAR TRANSCRIPT PROCESSING 90*, *OTP90*) caused premature stop codons (Table S3). In addition, a missense mutation was identified in AT1G24300 (a GYF domain-containing protein), which is a homolog of *Essential for poteXvirus Accumulation 1* (*EXA1*).

We attempted to map *es2s-3-4* by outcrossing two of its selfed alleles to *Ler*, but were unable to identify a nonrecombinant chromosomal region in the F_2 mapping population that displayed an ES2-hypersensitive phenotype (Figure S4).

es2s-3-6 was mapped to the right arm of chromosome 5, between positions 16–20.5 Mbp (Figure S5). Within this interval, there were SNPs in four candidate genes, as listed in Table S4.

es2s-6-3, *es2s-6-4*, and *es2s-6-7* were mapped to the same region at the left arm of chromosome 1, between 8.5 and 11.0 Mbp (Figures S6–S8). WGS of the F_2 mapping populations showed that these three mutants contained the same set of SNPs in this chromosomal region, suggesting they were allelic mutants (Table S5). In total, there were SNPs in 10 candidate genes in *es2s-6-3*, *es2s-6-4*, and *es2s-6-7*. Notably, a missense mutation was identified in AT1G26110 (*DECAPPING5*, *DCP5*).

es2s-6-13 was likely mapped to the right terminus of chromosome 3, between 18.0 and 23.5 Mbp (Figure S9). The candidate interval was not clean, probably due to contamination when selecting seedlings. Within this interval, there were 11 candidate SNPs in 10 genes (Table S6). Four of the SNPs were annotated to be synonymous substitutions that did not change the amino acid coded. Nevertheless, these four synonymous mutations were marked as candidate SNPs because they might create new splicing sites or be target sites of micro RNAs.

es2s-10-2 was mapped to the right terminus of chromosome 1, between 26.5 and 30.4 Mbp (Figure S10). Within this interval, there were 10 SNPs in nine candidate genes (Table S7). *es2s-19-2* was also mapped to this region with the same set of SNPs, with the backcross strategy (Figure S16 and Table S7).

es2s-10-16 was mapped to the right arm of chromosome 5 (Figure S11), with SNPs in 11 candidate genes (Table S8).

es2s-12-5 was likely mapped to the right terminus of chromosome 2, between 15 and 19.7 Mbp (Figure S12). This interval was not clean, with the presence of *Ler* chromosomal content in the pooled F_2 seedlings. There were 7 candidate SNPs in this interval, but the confidence level was modest (Table S9).

es2s-15-12 was first mapped to the right arm of chromosome 2, but the interval was too wide. To increase the recombination, we pooled more than 300 F_2 seedlings displaying ES2-hypersensitive phenotype and sequenced again. The causal mutation was narrowed down to the 14.0- to 17.5-Mbp interval on chromosome 2 (Figure S14). Within this interval, there were five candidate SNPs (Table S10). Notably, there was a SNP in AT2G37500, encoding ArgJ, an enzyme in the arginine biosynthesis pathway.

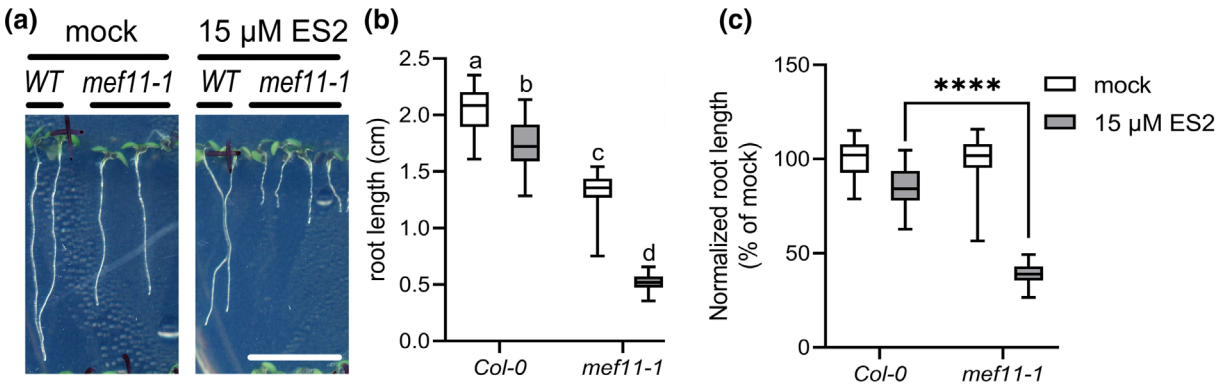

FIGURE 4 *mef11-1* is hypersensitive to ES2 for root growth inhibition. (a) Six-day-old light-grown seedlings of *Col-0* and *mef11-1* (SALK_061056) grown on plates containing mock or 15-μM ES2 treatment. Scale bar = 1 cm. Representative seedlings were shown. (b) Box plot of root lengths for 6-day-old seedlings shown in a, with whiskers displaying the minimum and maximum root length in each group. Statistical analysis was performed with two-way ANOVA, with Tukey's post hoc multiple comparisons among all groups. Letters denote statistical significance groups, with $p < 0.0001$. (c) Normalized root length for 6-day-old seedlings shown in a. Root length was normalized by dividing the average root length of mock treatment for each genotype and expressed as % of mock. Statistical analysis was performed with two-way ANOVA, with Tukey's post hoc multiple comparisons among all groups. **** denotes $p < 0.0001$. $N = 33–40$ seedlings in each group.

TABLE 3 Summary of T-DNA insertion alleles displaying an ES2-hypersensitive phenotype for root growth inhibition.

es2s allele	Candidate gene ID	Gene name	T-DNA insertion alleles
es2s-6-3/6-4/6-7	AT1G26110	*DECAPPING 5 (DCP5)*	SALK_063362C
es2s-10-2	AT1G80360	*INDOLE-SEVERE-SENSITIVE1 (ISS1)*	SAIL_576_D12; SAIL_134_C01
es2s-15-12	AT2G37500	Arginine biosynthesis protein *ArgJ*	SALK_066479C
es2s-15-9/16-5	AT4G14850	*MITOCHONDRIAL RNA EDITING FACTOR 11 (MEF11)*	SALK_061056C

es2s-18-1 was mapped to the left arm of chromosome 1, in the 7.0- to 10.0-Mbp interval (Figure S15). Interestingly, some of the SNPs overlapped with SNPs in other independent *es2s* lines (Table S11).

For *es2s-19-11*, we first attempted to map the mutant with the outcross strategy. However, a nonrecombinant region was not identified in the outcross mapping population. Subsequently, a backcross mapping strategy was employed. In the F2 population of the backcross line, mutant-like and wild type-like seedlings were pooled and sequenced separately. EMS-induced SNPs were used as markers in the computational genomics analysis to compare the genomic content between the mutant-like pool and wild type-like pool to map the causal mutation. Because the EMS-induced SNPs between the mutant and background line were more infrequent than the natural SNP variations between *Col-0* and *Ler* ecotypes, the resolution of backcross mapping was lower than outcross mapping, thus resulting in a larger chromosomal interval. In this mutant, the causal mutation was mapped to the left terminus of chromosome 5, between 0 and 6 Mbp, with the most likely interval at 3 and 5 Mbp (Figure S17). The candidate SNPs are listed in Table S12. Notably, there was a C to T missense mutation of *CELLULOSE SYNTHASE 5* (*CESA5*, AT5G09870) identified in this mutant at the position 3076482 of chromosome 5, resulting in an alanine to valine mutation at residue 677 of CESA5 (Table S12). This mutation fell into the intrinsically disordered "class specific region" (CSR) of CESA5.

Using the backcross strategy, *es2s-33-7* was mapped to the 6- to 10-Mbp interval of chromosome 1, with the most likely interval at 7–9 Mbp (Figure S18). The candidate SNPs are listed in Table S13.

3.5 | Identification of causal mutations by testing alternative alleles

To identify the causal mutation for each ES2-hypersensitive mutant, we obtained T-DNA insertion lines for numerous candidate genes as alternative alleles (illustrated in Figure 2c and summarized in Data Set 1). The T-DNA insertion lines were sowed on plates with mock, 15-μM ES2, or 25-μM ES2, to test for an ES2-hypersensitive phenotype. Using this strategy, an alternative allele for one of the candidate genes in *es2s-16-5*, *MITOCHONDRIAL RNA EDITING FACTOR 11 (MEF11)*, was identified. A T-DNA insertion mutant of *MEF11*, SALK_061056C (*mef11-1*), displayed an ES2-hypersensitive response for root growth inhibition (Figure 4).

Among the 139 T-DNA insertion lines tested so far, four additional T-DNA insertion mutants in three different genes displayed obvious ES2-hypersensitive phenotypes: SALK_063362C (*DECAPPING 5* [*DCP5*], AT1G26110), SAIL_576_D12 and SAIL_134_C01 (*INDOLE SEVERE SENSITIVE1* [*ISS1*] */REVERSAL OF SAV3 PHENOTYPE 1* [*VAS1*], AT1G80360), and SALK_066479C (Arginine biosynthesis

protein *ArgJ*, AT2G37500) (Table 3). All T-DNA insertion lines tested are listed in Data Set 1.

4 | DISCUSSION

In this study, we established an ES2 dose–response curve for root growth of wild-type *PIN2-GFP* and *Col-0* seedlings and found that 15- to 25-μM ES2 caused modest root growth inhibition in both lines. We used this concentration range as low-dose ES2 treatment for screening ES2-hypersensitive seedlings in an EMS-mutagenized *PIN2-GFP* population. With a two-round screening strategy, we discarded seedlings with intrinsic growth defects and only retained seedlings displaying growth defects upon ES2 treatment. More than 70 *es2s* mutants were identified from our screen. Using a pipeline of outcrossing/backcrossing combined with whole-genome sequencing, we mapped 18 *es2s* mutants to chromosomal regions harboring the causal mutations, of which 14 were nonallelic to each other. The screening and mapping pipeline developed in this study could be easily translated into hypersensitive mutant screens for hormones or other synthetic molecules.

The ES2-hypersensitive screen hit several genes that genetically and/or physically interact with exocyst subunits. For instance, we identified an A1220V single amino acid replacement of MYOSIN XI-1 (AT1G17580) in *es2s-2-19*, a nonsense mutation of FORMIN HOMOLOGUE 4 (FH4, AT1G24150) in *es2s-2-29*, and an A677V single amino acid replacement of CELLULOSE SYNTHASE 5 (CESA5; AT5G09870) in *es2s-19-11*, informing the possible role of cytoskeletal proteins and cargo proteins during the vesicle tethering step of exocytosis. In addition, *DCP5* (*DECAPPING PROTEIN 5*, AT1G26110) was identified as a candidate SNP, which encodes a protein required for mRNA decapping, RNA processing body (P body) formation, and translational repression (Hoffmann et al., 2022; Jang et al., 2019; Wang et al., 2023). Interestingly, DCP5 and its binding partner DCP1 were recently shown to be involved in the formation of cellular condensates and actin remodeling, independent of its mRNA decapping function (Liu et al., 2023).

There were also genes involved in response to pathogens identified as candidate SNPs. For example, previous research reported that *Essential for poteXvirus Accumulation 1* (*EXA1*), encoding a GYF domain protein, facilitated Potexvirus infection in Arabidopsis (Hashimoto et al., 2016; Nishikawa et al., 2023). Loss of function of *EXA1* conferred resistance to Potexvirus. Considering the involvement of exocyst complex in pathogen infections (Du et al., 2018; Pečenková et al., 2011), the identification of AT1G24300, a homolog of *EXA1*, in *es2s-29* could be relevant.

For the candidate genes in *es2s* mutants, we employed a strategy to test T-DNA insertion lines as alternative alleles. Due to the substantial number of candidate genes and subsequently the large number of individual T-DNA insertion lines to be tested, our strategy was to directly sow the seeds received from the Arabidopsis Biological Resources Center (ABRC) on plates for mock and low-dose ES2 treatment. Lines that displayed ES2 hypersensitive phenotypes or segregating phenotypes were propagated and genotyped, whereas lines with wild-type phenotype were not pursued further. This strategy has high positive predictive value but low sensitivity as some of the nonsensitive lines could be due to wild-type or heterozygous genotype of seeds obtained from ABRC. With this strategy, we identified several alternative alleles for *es2s* mutants. For candidate genes in *es2s-6-3/6-4/6-7*, one T-DNA insertion line for *DCP5* (AT1G26110) displayed a hypersensitive response to ES2, confirming this as the causal mutation at this locus. For *es2s-10-2*, two T-DNA insertion lines for *VAS1/ISS1* (AT1G80360) displayed a hypersensitive response to ES2. *VAS1/ISS1* encodes a methionine-specific aminotransferase, which transfers the amino group from the ethylene biosynthetic intermediate methionine to the auxin biosynthetic intermediate indole-3-pyruvic acid (Zheng et al., 2013). For *es2s-15-12*, we identified a T-DNA insertion mutant of *ArgJ* (AT2G37500) that mimicked the ES2-hypersensitive phenotype. *ArgJ* encodes an acetyltransferase in the arginine biosynthesis pathway (Buchanan et al., 2015). For *es2s-16-5*, a T-DNA insertion mutant of *MEF11/LOI1* (AT4G14850) exhibited an ES2-hypersensitive phenotype. *MEF11/LOI1* encodes MITOCHONDRIAL RNA EDITING FACTOR 11, which is a pentatricopeptide (PPR) protein that binds single-stranded RNA (Kobayashi et al., 2007; Verbitskiy et al., 2010). The functional characterization of ES2-hypersensitive mutants identified in this study is in progress.

Alternatively, a genetic complementation strategy could be used to identify the causal mutation among the many candidate genes, by preparing a wild-type genetic complementation construct for each candidate gene and transforming into the mutant *es2s* lines. The genetic complementation strategy is more reliable than testing T-DNA insertion mutants, as knockout or knockdown caused by T-DNA insertions can have different consequences than single amino acid replacement caused by EMS mutagenesis. However, in our case, this strategy presented practical challenges as we were dealing with more than 130 candidate genes among the mapped mutants. Moreover, some of the genes were more than 10 kb in length, making vector construction challenging.

Another alternative strategy to identify the causal mutation is to repeatedly backcross the mutants for several generations. Multiple backcrosses could increase gene recombination, remove irrelevant mutations, and narrow down the interval harboring the causal mutation.

A lesson we learned from this screen is to have a proper balance of SNP density in each mutant, by controlling the strength of EMS mutagenesis. To cover as many genes as possible, we used a moderately potent EMS treatment for mutagenesis. This led to multiple SNPs in each chromosomal interval during mapping analysis and made causal mutation identification challenging. Considering that the work during mutant screening is repetitive and easy to scale up, whereas the process of causal mutation identification is complicated and difficult to scale up, it would be prudent to use a low potency of EMS mutagenesis and screen more seedlings to lessen the burden of causal mutation identification.

Considering the systematic approach we employed for mutant screening, we expected to identify a diverse range of genes that were

closely or remotely related to the exocyst. From the candidate genes list, we found a wide range of genes. Although we did not identify mutants with a known hypersensitive response to ES2 like *scd1*, *scd2*, or *nerd1* in the currently mapped *es2s* mutants, nor did we hit any exocyst subunits, these could be present in the large collection of *es2s* mutants that have not been mapped yet. We did the screening and mapping in multiple batches, while constantly optimizing and tailoring our approaches during the study. There were several promising *es2s* mutants with a strong ES2-hypersensitive phenotype that have not been mapped yet. Alternatively, it is possible that ES2—as a small synthetic molecule—could have targets other than EXO70A1, thus leading to some hypersensitive mutants not related to exocytosis defects.

A promising future research direction involves further characterization of the *es2s* mutants by assessing their response to effectors that target the exocyst complex. For instance, AVR-Pii, an effector secreted by *Magnaporthe oryzae*, targets the *EXO70F* subunit (De la Concepcion et al., 2022). Transforming AVR-Pii driven by an inducible promoter into Arabidopsis wild type and *es2s* mutants, and assessing the sensitivity of *es2s* mutants to the expression of AVR-Pii, could reveal further the relevance of *es2s* mutants to exocyst function. In addition, given the critical role of exocyst in delivering the Cellulose Synthase Complex (CSC) to the PM (Zhang et al., 2021; Zhu et al., 2018), the *es2s* lines could be subjected to cellulose biosynthesis inhibitors and evaluated for their sensitivity to cellulose synthesis inhibition.

Beyond studies of exocytosis, these EMS mutants identified and mapped in this study have broader impacts, as they serve as useful genetic resources for future studies. There are single amino acid replacement mutations and premature stop codon mutations for several genes of interest for other studies. Thus, other researchers interested in these genes could clean up the background mutations through backcrossing and use for their studies.

AUTHOR CONTRIBUTIONS

Chunhua Zhang, Xiaohui Li, and Christopher J. Staiger conceived the project and designed the experiments. Xiaohui Li and Christopher J. Staiger wrote the manuscript. Diwen Wang participated in the mutant screening and mapping, as well as the preparation of Figure 2. Xianglin Yin synthesized ES2. Mingji Dai supervised the synthesis of ES2. Xiaohui Li performed all other experiments and prepared the figures, unless otherwise stated.

ACKNOWLEDGMENTS

This paper is dedicated to the memory of Dr. Chunhua Zhang, who passed away on May 15, 2021, after a brave fight with cancer. Dr. Zhang originally conceived this project and was a great mentor, friend, and colleague. We acknowledge Monica A. Haughan for participating in the mutant screening during her time as an undergraduate research assistant at Purdue University. The authors thank current and previous members of the Staiger/C. Zhang laboratory for helpful discussions and critical comments, especially Drs. Lei Huang and Weiwei Zhang. We appreciate Dr. Xiang Liu from the Department of Computer and Information Technology, Purdue University, for installation of UNIX packages. We acknowledge the Purdue Genomics Core Facility for providing sequencing services for a subset of the mutants, and we thank Drs. Brian Dilkes and Phillip SanMiguel from Purdue for helpful discussions regarding mutant mapping.

CONFLICT OF INTEREST STATEMENT

The authors declare no conflict of interest.

PEER REVIEW

The peer review history for this article is available in the Supporting Information for this article.

DATA AVAILABILITY STATEMENT

Data supporting this manuscript are included as tables, figures, or supporting information.

ORCID

Xiaohui Li https://orcid.org/0000-0002-0012-8018
Diwen Wang https://orcid.org/0000-0002-0667-3121
Xianglin Yin https://orcid.org/0000-0003-4549-0827
Mingji Dai https://orcid.org/0000-0001-7956-6426
Christopher J. Staiger https://orcid.org/0000-0003-2321-1671
Chunhua Zhang https://orcid.org/0000-0003-0985-7185

REFERENCES

Aniento, F., Sánchez de Medina Hernández, V., Dagdas, Y., Rojas-Pierce, M., & Russinova, E. (2022). Molecular mechanisms of endomembrane trafficking in plants. *The Plant Cell*, *34*, 146–173. https://doi.org/10.1093/plcell/koab235

Austin, R. S., Chatfield, S. P., Desveaux, D., & Guttman, D. S. (2014). Next-generation mapping of genetic mutations using bulk population sequencing. In J. J. Sanchez-Serrano & J. Salinas (Eds.), *Methods in molecular biology. Arabidopsis protocols* (pp. 301–315). Humana Press. https://doi.org/10.1007/978-1-62703-580-4_17

Austin, R. S., Vidaurre, D., Stamatiou, G., Breit, R., Provart, N. J., Bonetta, D., Zhang, J., Fung, P., Gong, Y., Wang, P. W., McCourt, P., & Guttman, D. S. (2011). Next-generation mapping of Arabidopsis genes. *The Plant Journal*, *67*, 715–725. https://doi.org/10.1111/j.1365-313X.2011.04619.x

Battey, N. H., James, N. C., Greenland, A. J., & Brownlee, C. (1999). Exocytosis and endocytosis. *The Plant Cell*, *11*, 643–659. https://doi.org/10.1105/tpc.11.4.643

Buchanan, B. B., Gruissem, W., & Jones, R. L. (Eds.). (2015). *Biochemistry & molecular biology of plants*. John Wiley & Sons Inc.

Chen, X., & Friml, J. (2014). Rho-GTPase-regulated vesicle trafficking in plant cell polarity. *Biochemical Society Transactions*, *42*, 212–218. https://doi.org/10.1042/BST20130269

Cole, R. A., Peremyslov, V. V., Van Why, S., Moussaoui, I., Ketter, A., Cool, R., Moreno, M. A., Vejlupkova, Z., Dolja, V. V., & Fowler, J. E. (2018). A broadly conserved NERD genetically interacts with the exocyst to affect root growth and cell expansion. *Journal of Experimental Botany*, *69*, 3625–3637. https://doi.org/10.1093/jxb/ery162

Cvrčková, F., Grunt, M., Bezvoda, R., Hála, M., Kulich, I., Rawat, A., & Žárský, V. (2012). Evolution of the land plant exocyst complexes. *Frontiers in Plant Science*, *3*, 159. https://doi.org/10.3389/fpls.2012.00159

De la Concepcion, J. C., Fujisaki, K., Bentham, A. R., Cruz Mireles, N., Sanchez de Medina Hernandez, V., Shimizu, M., Lawson, D. M., Kamoun, S., Terauchi, R., & Banfield, M. J. (2022). A blast fungus

zinc-finger fold effector binds to a hydrophobic pocket in host Exo70 proteins to modulate immune recognition in rice. *Proceedings of the National Academy of Sciences*, *119*, e2210559119. https://doi.org/10.1073/pnas.2210559119

Drakakaki, G., Robert, S., Szatmari, A.-M., Brown, M. Q., Nagawa, S., van Damme, D., Leonard, M., Yang, Z., Girke, T., Schmid, S. L., Russinova, E., Friml, J., Raikhel, N. V., & Hicks, G. R. (2011). Clusters of bioactive compounds target dynamic endomembrane networks in vivo. *Proceedings of the National Academy of Sciences*, *108*, 17850–17855. https://doi.org/10.1073/pnas.1108581108

Drdová, E. J., Synek, L., Pečenková, T., Hála, M., Kulich, I., Fowler, J. E., Murphy, A. S., & Žárský, V. (2013). The exocyst complex contributes to PIN auxin efflux carrier recycling and polar auxin transport in Arabidopsis. *The Plant Journal*, *73*, 709–719. https://doi.org/10.1111/tpj.12074

Du, Y., Overdijk, E. J. R., Berg, J. A., Govers, F., & Bouwmeester, K. (2018). Solanaceous exocyst subunits are involved in immunity to diverse plant pathogens. *Journal of Experimental Botany*, *69*, 655–666. https://doi.org/10.1093/jxb/erx442

Elias, M., Drdová, E., Ziak, D., Bavlnka, B., Hála, M., Cvrčková, F., Soukupova, H., & Žárský, V. (2003). The exocyst complex in plants. *Cell Biology International*, *27*, 199–201. https://doi.org/10.1016/S1065-6995(02)00349-9

Friml, J. (2010). Subcellular trafficking of PIN auxin efflux carriers in auxin transport. *European Journal of Cell Biology*, *89*, 231–235. https://doi.org/10.1016/j.ejcb.2009.11.003

Hashimoto, M., Neriya, Y., Keima, T., Iwabuchi, N., Koinuma, H., Hagiwara-Komoda, Y., Ishikawa, K., Himeno, M., Maejima, K., Yamaji, Y., & Namba, S. (2016). EXA1, a GYF domain protein, is responsible for loss-of-susceptibility to plantago asiatica mosaic virus in *Arabidopsis thaliana*. *The Plant Journal*, *88*, 120–131. https://doi.org/10.1111/tpj.13265

Heider, M. R., & Munson, M. (2012). Exorcising the exocyst complex. *Traffic*, *13*, 898–907. https://doi.org/10.1111/j.1600-0854.2012.01353.x

Hoffmann, G., Mahboubi, A., Bente, H., Garcia, D., Hanson, J., & Hafrén, A. (2022). Arabidopsis RNA processing body components LSM1 and DCP5 aid in the evasion of translational repression during *Cauliflower mosaic virus* infection. *The Plant Cell*, *34*, 3128–3147. https://doi.org/10.1093/plcell/koac132

Ischebeck, T., Werner, S., Krishnamoorthy, P., Lerche, J., Meijón, M., Stenzel, I., Löfke, C., Wiessner, T., Im, Y. J., Perera, I. Y., Iven, T., Feussner, I., Busch, W., Boss, W. F., Teichmann, T., Hause, B., Persson, S., & Heilmann, I. (2014). Phosphatidylinositol 4,5-bisphosphate influences PIN polarization by controlling clathrin-mediated membrane trafficking in *Arabidopsis*. *The Plant Cell*, *25*, 4894–4911. https://doi.org/10.1105/tpc.113.116582

Jang, G.-J., Yang, J.-Y., Hsieh, H.-L., & Wu, S.-H. (2019). Processing bodies control the selective translation for optimal development of Arabidopsis young seedlings. *Proceedings of the National Academy of Sciences*, *116*, 6451–6456. https://doi.org/10.1073/pnas.1900084116

Kim, Y., Schumaker, K. S., & Zhu, J.-K. (2006). EMS mutagenesis of *Arabidopsis*. In *Arabidopsis protocols* (pp. 101–104). Humana Press.

Kleine-Vehn, J., Wabnik, K., Martinière, A., Łangowski, Ł., Willig, K., Naramoto, S., Leitner, J., Tanaka, H., Jakobs, S., Robert, S., Luschnig, C., Govaerts, W., W Hell, S., Runions, J., & Friml, J. (2011). Recycling, clustering, and endocytosis jointly maintain PIN auxin carrier polarity at the plasma membrane. *Molecular Systems Biology*, *7*, 540. https://doi.org/10.1038/msb.2011.72

Kobayashi, K., Suzuki, M., Tang, J., Nagata, N., Ohyama, K., Seki, H., Kiuchi, R., Kaneko, Y., Nakazawa, M., Matsui, M., Matsumoto, S., Yoshida, S., & Muranaka, T. (2007). LOVASTATIN INSENSITIVE 1, a novel pentatricopeptide repeat protein, is a potential regulatory Factor of isoprenoid biosynthesis in Arabidopsis. *Plant and Cell Physiology*, *48*, 322–331. https://doi.org/10.1093/pcp/pcm005

Langmead, B., & Salzberg, S. L. (2012). Fast gapped-read alignment with Bowtie 2. *Nature Methods*, *9*, 357–359. https://doi.org/10.1038/nmeth.1923

Larson, E. R., Ortmannová, J., Donald, N. A., Alvim, J., Blatt, M. R., & Žárský, V. (2020). Synergy among exocyst and SNARE interactions identifies a functional hierarchy in secretion during vegetative growth. *The Plant Cell*, *32*, 2951–2963. https://doi.org/10.1105/tpc.20.00280

Lešková, A., Labajová, M., Krausko, M., Zahradníková, A., Baluška, F., Mičieta, K., Turňa, J., & Jásik, J. (2020). Endosidin 2 accelerates PIN2 endocytosis and disturbs intracellular trafficking of PIN2, PIN3, and PIN4 but not of SYT1. *PLoS ONE*, *15*, e0237448. https://doi.org/10.1371/journal.pone.0237448

Li, H., Handsaker, B., Wysoker, A., Fennell, T., Ruan, J., Homer, N., Marth, G., Abecasis, G., Durbin, R., & 1000 Genome Project Data Processing Subgroup. (2009). The sequence alignment/map format and SAMtools. *Bioinformatics*, *25*, 2078–2079.

Li, X., Zhu, P., Chen, Y.-J., Huang, L., Wang, D., Newton, D. T., Hsu, C. C., Lin, G., Tao, W. A., Staiger, C. J., & Zhang, C. (2023). The EXO70 inhibitor Endosidin2 alters plasma membrane protein composition in Arabidopsis roots. *Frontiers in Plant Science*, *14*, 1171957. https://doi.org/10.3389/fpls.2023.1171957

Liu, C., Mentzelopoulou, A., Muhammad, A., Volkov, A., Weijers, D., Gutierrez-Beltran, E., & Moschou, P. N. (2023). An actin remodeling role for *Arabidopsis* processing bodies revealed by their proximity interactome. *The EMBO Journal*, *42*, e111885. https://doi.org/10.15252/embj.2022111885

Luschnig, C., & Vert, G. (2014). The dynamics of plant plasma membrane proteins: PINs and beyond. *Development*, *141*, 2924–2938. https://doi.org/10.1242/dev.103424

Mayers, J. R., Hu, T., Wang, C., Cárdenas, J. J., Tan, Y., Pan, J., & Bednarek, S. Y. (2017). SCD1 and SCD2 form a complex that functions with the exocyst and RabE1 in exocytosis and cytokinesis. *The Plant Cell*, *29*, 2610–2625. https://doi.org/10.1105/tpc.17.00409

Mei, K., Li, Y., Wang, S., Shao, G., Wang, J., Ding, Y., Luo, G., Yue, P., Liu, J. J., Wang, X., Dong, M. Q., Wang, H. W., & Guo, W. (2018). Cryo-EM structure of the exocyst complex. *Nature Structural & Molecular Biology*, *25*, 139–146. https://doi.org/10.1038/s41594-017-0016-2

Nishikawa, M., Katsu, K., Koinuma, H., Hashimoto, M., Neriya, Y., Matsuyama, J., Yamamoto, T., Suzuki, M., Matsumoto, O., Matsui, H., & Nakagami, H. (2023). Interaction of EXA1 and eIF4E family members facilitates potexvirus infection in Arabidopsis thaliana. *Journal of Virology*, *97*, e00221-23.

Pečenková, T., Hála, M., Kulich, I., Kocourková, D., Drdová, E., Fendrych, M., Toupalová, H., & Žárský, V. (2011). The role for the exocyst complex subunits Exo70B2 and Exo70H1 in the plant–pathogen interaction. *Journal of Experimental Botany*, *62*, 2107–2116. https://doi.org/10.1093/jxb/erq402

Verbitskiy, D., Zehrmann, A., Brennicke, A., & Takenaka, M. (2010). A truncated MEF11 protein shows site-specific effects on mitochondrial RNA editing. *Plant Signaling & Behavior*, *5*, 558–560. https://doi.org/10.4161/psb.11095

Wang, W., Wang, C., Wang, Y., Ma, J., Wang, T., Tao, Z., Liu, P., Li, S., Hu, Y., Gu, A., Wang, H., Qiu, C., & Li, P. (2023). The P-body component DECAPPING5 and the floral repressor SISTER OF FCA regulate *FLOWERING LOCUS C* transcription in Arabidopsis. *The Plant Cell*, *35*, 3303–3324. https://doi.org/10.1093/plcell/koad151

Wilson, P. R., Ganguly, D., Hou, X., & Pogson, B. (2018). CTAB genomic DNA extraction from Arabidopsis leaf material v2.

Xu, J., & Scheres, B. (2005). Dissection of Arabidopsis ADP-RIBOSYLATION FACTOR 1 function in epidermal cell polarity. *The Plant Cell*, *17*, 525–536. https://doi.org/10.1105/tpc.104.028449

Zavaliev, R., Levy, A., Gera, A., & Epel, B. L. (2013). Subcellular dynamics and role of *Arabidopsis* β-1,3-glucanases in cell-to-cell movement of

tobamoviruses. *Molecular Plant-Microbe Interactions*, *26*, 1016–1030. https://doi.org/10.1094/MPMI-03-13-0062-R

Zhang, C., Brown, M. Q., van de Ven, W., Zhang, Z. M., Wu, B., Young, M. C., Synek, L., Borchardt, D., Harrison, R., Pan, S., & Luo, N. (2016). Endosidin2 targets conserved exocyst complex subunit EXO70 to inhibit exocytosis. *Proceedings of the National Academy of Sciences*, *113*, E41–E50.

Zhang, L., Xing, J., & Lin, J. (2019). At the intersection of exocytosis and endocytosis in plants. *New Phytologist*, *224*, 1479–1489. https://doi.org/10.1111/nph.16018

Zhang, W., Cai, C., & Staiger, C. J. (2019). Myosins XI are involved in exocytosis of cellulose synthase complexes. *Plant Physiology*, *179*, 1537–1555. https://doi.org/10.1104/pp.19.00018

Zhang, W., Huang, L., Zhang, C., & Staiger, C. J. (2021). Arabidopsis myosin XIK interacts with the exocyst complex to facilitate vesicle tethering during exocytosis. *The Plant Cell*, *33*, 2454–2478. https://doi.org/10.1093/plcell/koab116

Zheng, Z., Guo, Y., Novák, O., Dai, X., Zhao, Y., Ljung, K., Noel, J. P., & Chory, J. (2013). Coordination of auxin and ethylene biosynthesis by the aminotransferase VAS1. *Nature Chemical Biology*, *9*, 244–246. https://doi.org/10.1038/nchembio.1178

Zhu, X., Li, S., Pan, S., Xin, X., & Gu, Y. (2018). CSI1, PATROL1, and exocyst complex cooperate in delivery of cellulose synthase complexes to the plasma membrane. *Proceedings of the National Academy of Sciences*, *115*, E3578–E3587.

Zhu, Y., & McFarlane, H. E. (2022). Regulation of cellulose synthesis via exocytosis and endocytosis. *Current Opinion in Plant Biology*, *69*, 102273. https://doi.org/10.1016/j.pbi.2022.102273

SUPPORTING INFORMATION

Additional supporting information can be found online in the Supporting Information section at the end of this article.

How to cite this article: Li, X., Wang, D., Yin, X., Dai, M., Staiger, C. J., & Zhang, C. (2024). A chemical genetic screen with the EXO70 inhibitor Endosidin2 uncovers potential modulators of exocytosis in Arabidopsis. *Plant Direct*, *8*(6), e592. https://doi.org/10.1002/pld3.592